

Supporting Information

New Evidence for a Quasi-Simultaneous Proton-Coupled Two-Electron Transfer and Direct Wiring for Glucose Oxidase Captured by the Carbon Nanotube- Polymer Matrix

Yiyang Liu,[†] Tinatin D. Dolidze^{§,‡}, Sameer Singhal[#] Dimitri E. Khoshtariya,^{‡,§} Jianjun Wei,^{†*}*

[†]Department of Nanoscience, Joint School of Nanoscience and Nanoengineering, University of North Carolina at Greensboro, Greensboro, NC 27401, USA. [‡]Institute for Biophysics and Bionanosciences, Department of Physics, I. Javakhishvili Tbilisi State University, Block II, 0128 Tbilisi, Georgian Republic. [§]Department of Biophysics, I. Beritashvili Center for Experimental Biomedicine, 0160 Tbilisi, Georgian Republic. [#]Biomedical & Energy Technology Branch, CFD Research Corporation, 701 McMillian Way NW, Huntsville, AL 35806, USA.

Atomic Force Microscopy (AFM): AFM was used to investigate the size changes and morphology of the SWCNT after the severe ultra-sonication. The CNT solution after sonication was diluted in DI water and then casted onto a freshly cleaved mica surface. The sample was kept at room temperature in a clean hood overnight to evaporate completely. The AFM images were obtained using Agilent Technologies 5600 LS Series Atomic Force Microscope equipped at JSNN. Figure 1S displays the AFM image of the CNT distributed at mica surfaces. The images show some aggregated clusters of the CNTs that display dimensions of 300-700 nm. Smaller pieces are also observed which could be the broken SWCNT fractions or contaminations from CNT sources. One have to note that

distribution of CNTs at mica surfaces should be different from that at the GC surface which is expected to be much more uniform. This particular image gives an idea solely on the average CNT size, not the distribution at GC electrode.

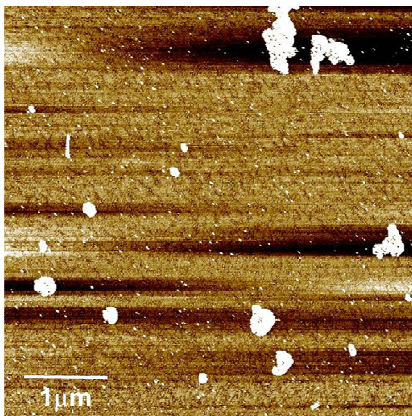


Figure S1. AFM images of the C-OOH functionalized single-walled CNT distributed on freshly cleaved mica surfaces. The white spots show the aggregated clusters of the SWCNTs

Cyclic Voltammetry of GOx at different types of electrodes.

Cyclic voltammetry was performed on GOx immobilized electrodes modified with a CNT/PEI matrix, CNT only, or PEI polymer only. Figure S2 shows voltammograms of the electrodes in a pH 7, 20 mM phosphate buffer solution at scan rate 50 mV/sec within potential window -0.7 V to 0 V vs. Ag/AgCl. The expanded nonfaradaic charging currents in voltammograms of CNT/GC and PEI/CNT/GC electrodes indicate the larger surface area of the electrode, as compared to the bare GC electrode. The PEI/CNT modified electrode displayed a slight increase of the charging current as compared to the CNT electrode, suggesting a minor contribution in the effective reaction surface area from polymer PEI.

In every case, when a modified electrode was placed directly in the electrochemical cell containing only the buffer solution (not exposed to GOx), the voltammogram displayed no faradaic response (data not shown). Subsequently, the same electrode was treated with GOx, rinsed, and placed in the buffer solution (see Experimental Section for details). In each case a well-defined faradaic response was observed for the electrodes that were incubated in the GOx solution. However, the Faradaic current of GOx on PEI/CNT/GC

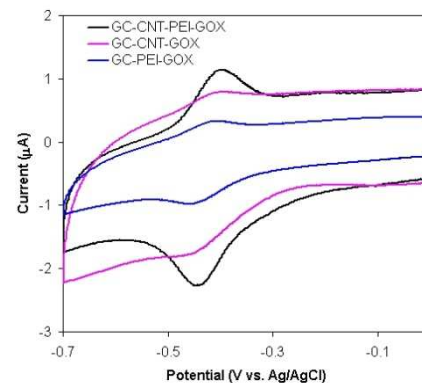
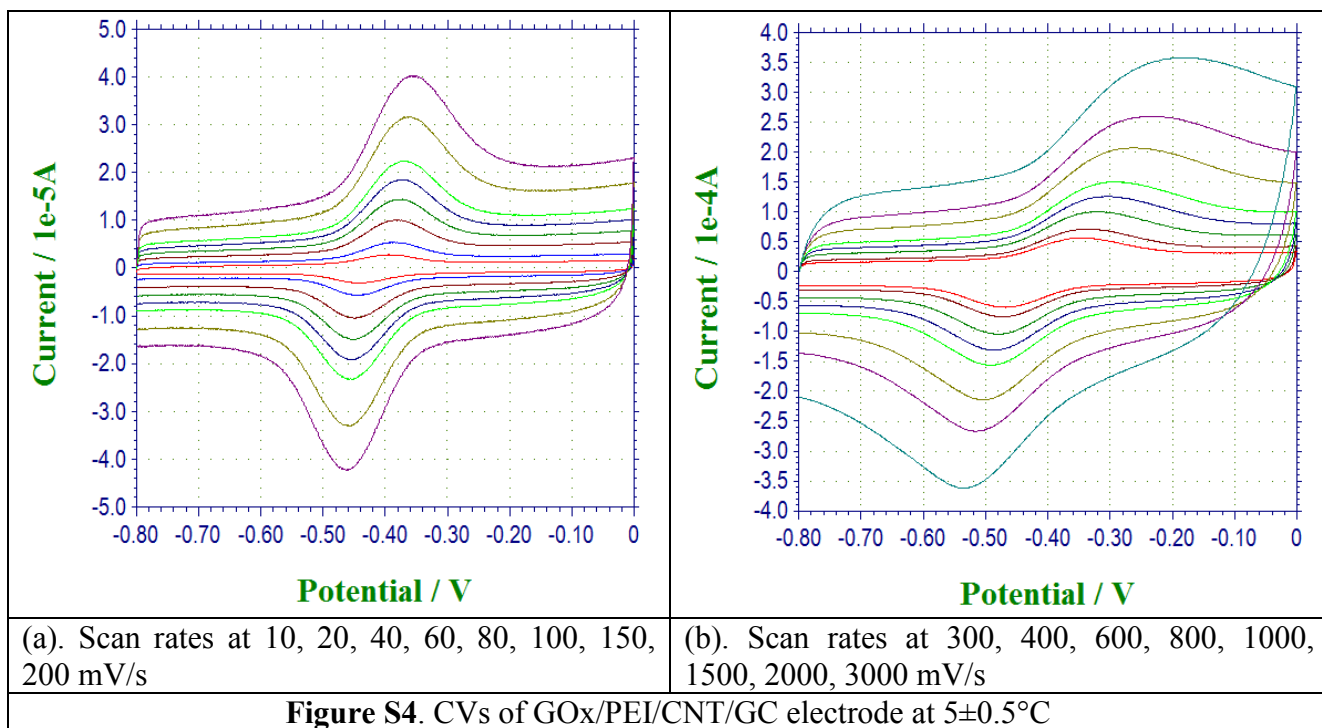
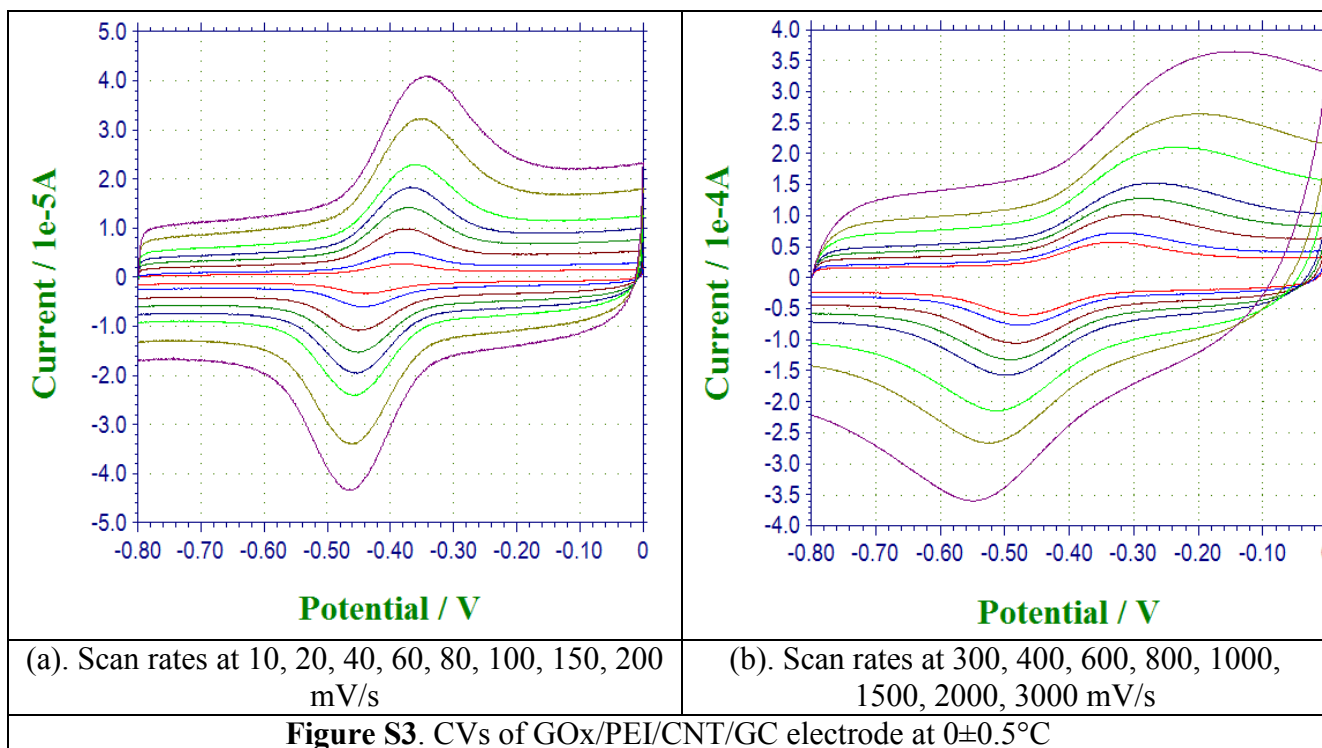
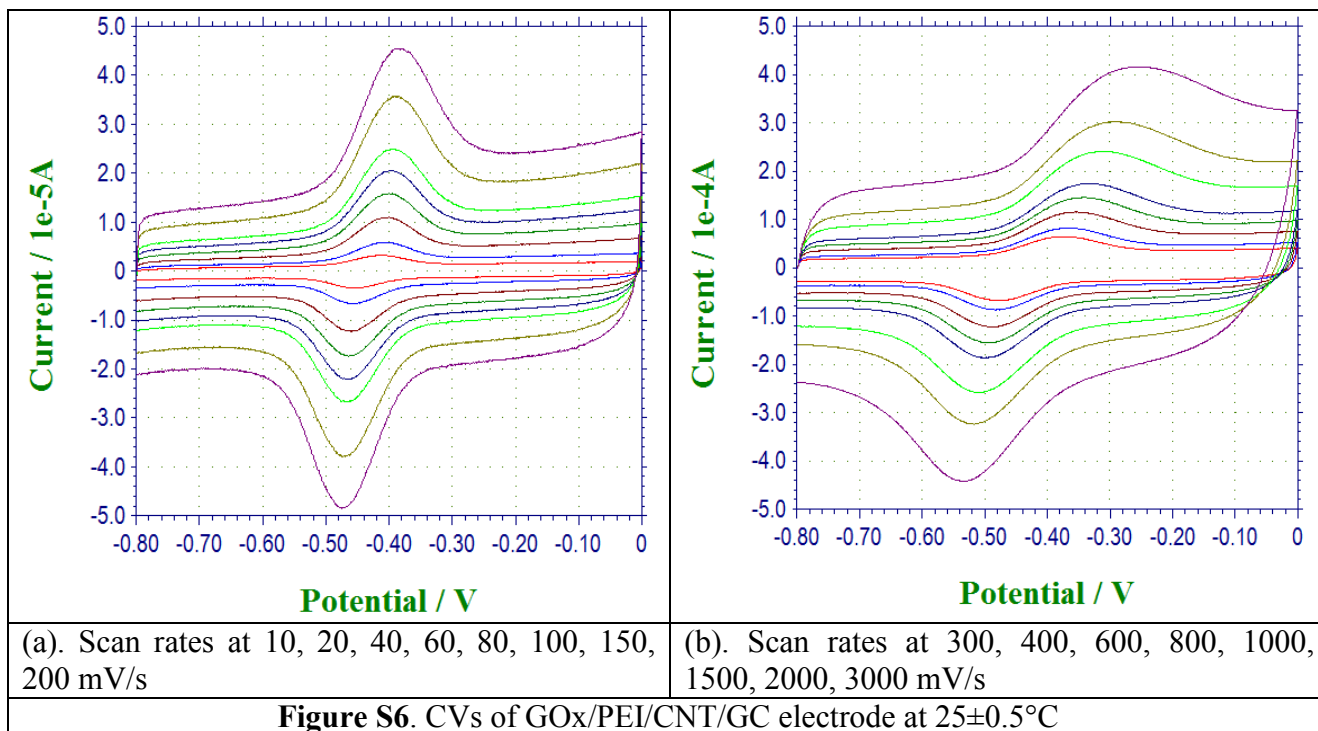
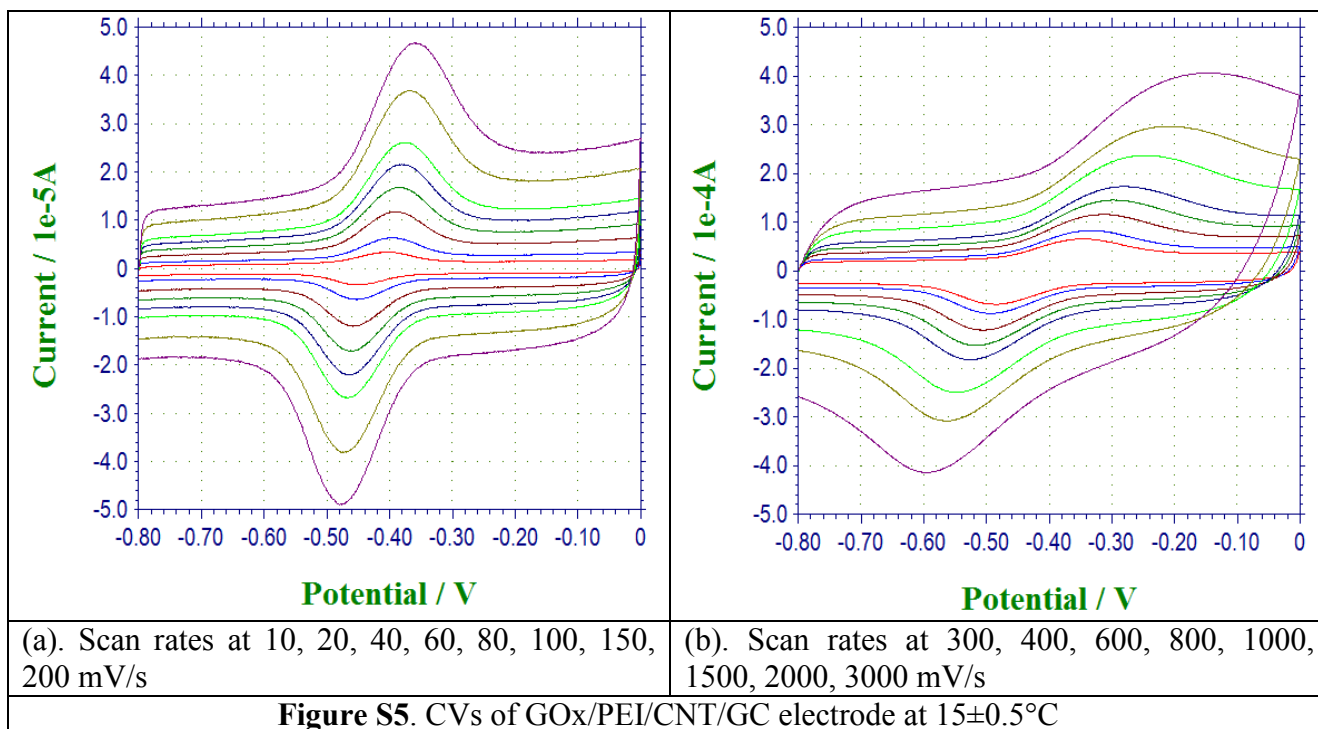


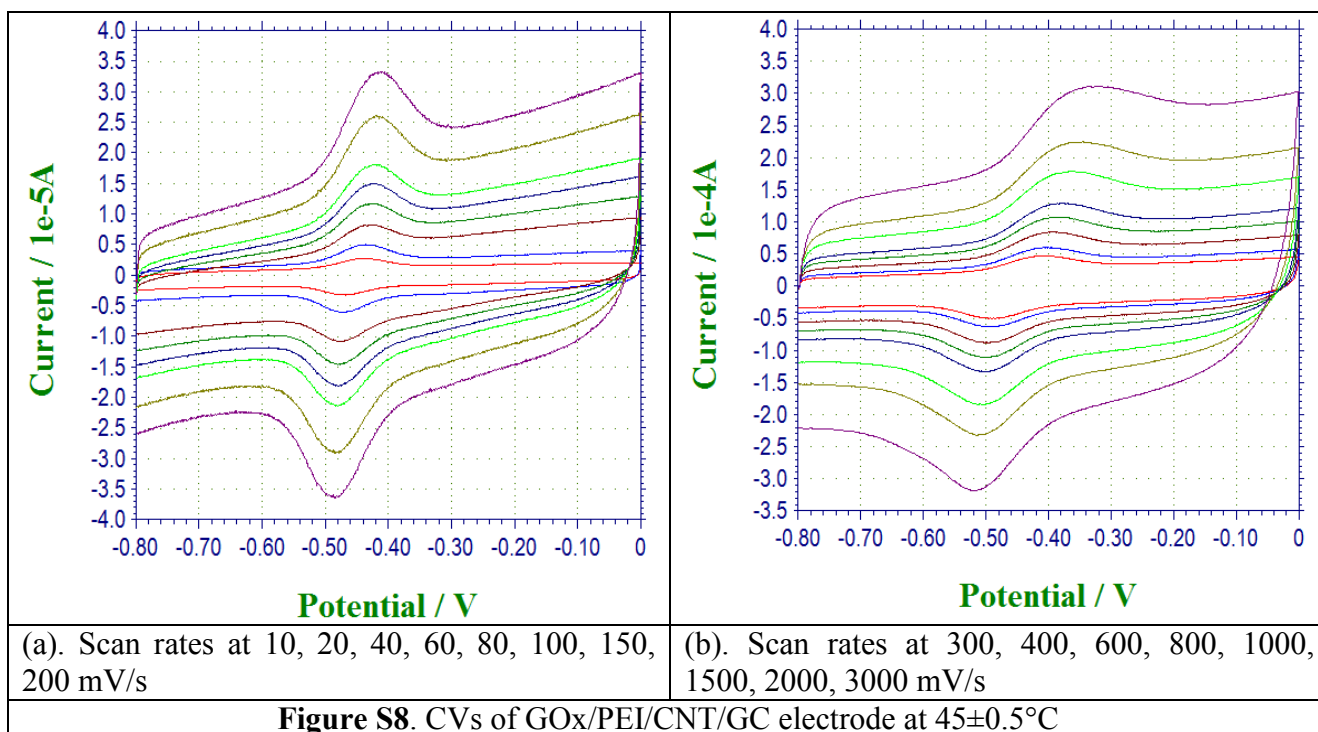
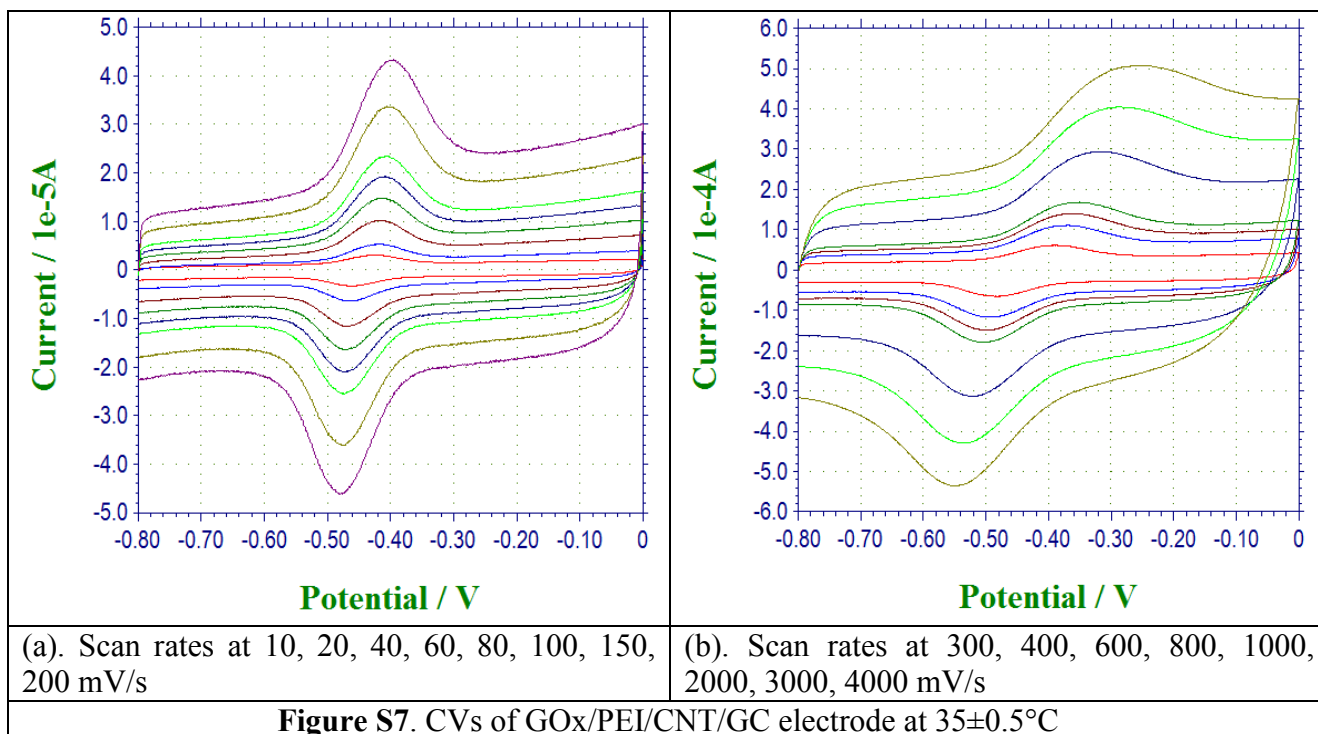
Figure S2. Representative cyclic voltammograms of glucose oxidase immobilized at CNT/PEI (black), PEI only (purple) and CNT only (blue) modified glassy carbon electrodes, respectively.

electrode is much more prominent than that on CNT/GC or PEI/GC electrode, implying that more GOx molecules were active and immobilized in the matrix and involved in the redox reaction at the PEI/CNT/GC electrode. It should be noted that non-Faradaic current was observed from the bare GC electrode after incubation in GOx solution. The electrochemical responses demonstrate the glucose oxidase (GOx) immobilization on the surface of differently modified GC electrodes.

Cyclic Voltamograms at different temperatures: The CV experiments were carried out in the temperature controlled water bath. The supporting electrolyte solution was purchased with a nitrogen gas stream for 10 min and maintain the N₂ at the top of electrochemical cell. Three electrodes were carried out at each temperatures. The representative CVs at individual temperatures are shown below.







Electrode Surface Area and Surface Coverage: In Figure S3, Panel A shows a typical voltammogram of GOx immobilized on a GC electrode coated with SWCNT/PEI matrix at scan rate 20 mV/s and in a pH 7 supporting electrolyte solution. It is possible to estimate the capacitive surface area from the nonfaradaic charge in the cyclic voltammograms by applying the ideal parallel-plate capacitor model,¹

$$A = C / K = \frac{\Delta I}{2\nu K}$$

where A represents the apparent capacitive surface area, ΔI is the charging current difference of positive and negative scan at a voltage having stable nonfaradaic current responses, ν is the scan rate, and K is the constant for the carbonaceous surface capacitance.² In electrochemical process, the electrode-solution interface in the absence of a redox couple can be simplified as a model of a pure parallel-plate capacitor, charge on the capacitor, Q , is proportional to the voltage drop across the capacitor, E , $Q=CE$, and then $\frac{dQ}{dt} = C \frac{dE}{dt}$, i.e. $i = C\nu$, ν is the scan rate of cyclic voltage scan rate.

The proportionality constant C is the capacitance of the medium. The simplest description of electrochemical capacitance is the Helmholtz model given by $\frac{C}{A} = \frac{\varepsilon\varepsilon_0}{l} = K$, where ε , ε_0 are the dielectric constant of the material separating the parallel plates and permittivity of free space, respectively, l is the separation between the plates (double layer thickness), and A is the area of the electrode. Assuming that l and ε , ε_0 are the same for all electrodes, the charging current is proportional to the electrode area exposed to the electrolyte solution. For our capacitive surface area, we used K value of 20×10^{-6} [F/cm²]. Panel B (Figure S3) plots the capacitive areas of the GOx/PEI/SWCNT/GC electrodes (0.6 μ L SWCNT-COOH loading for each electrode) as a function of the pH; the data are averaged from three electrodes for each pH experiment. Note that the

apparent geometrical area of the 3 mm diameter GC electrode is ca. 0.0707 cm^2 , the capacitive area of the GOx/PEI/SWCNT/GC electrodes are amplified by 30-40 times over that of the apparent geometrical area, in agreement with the findings by others.² This can be indicative of the “threading” phenomenon possibly involving a few of GOx biomolecules per one nanotube occurring over the fraction of SWCNTs that accidentally attain well-oriented positions versus the GC surface.

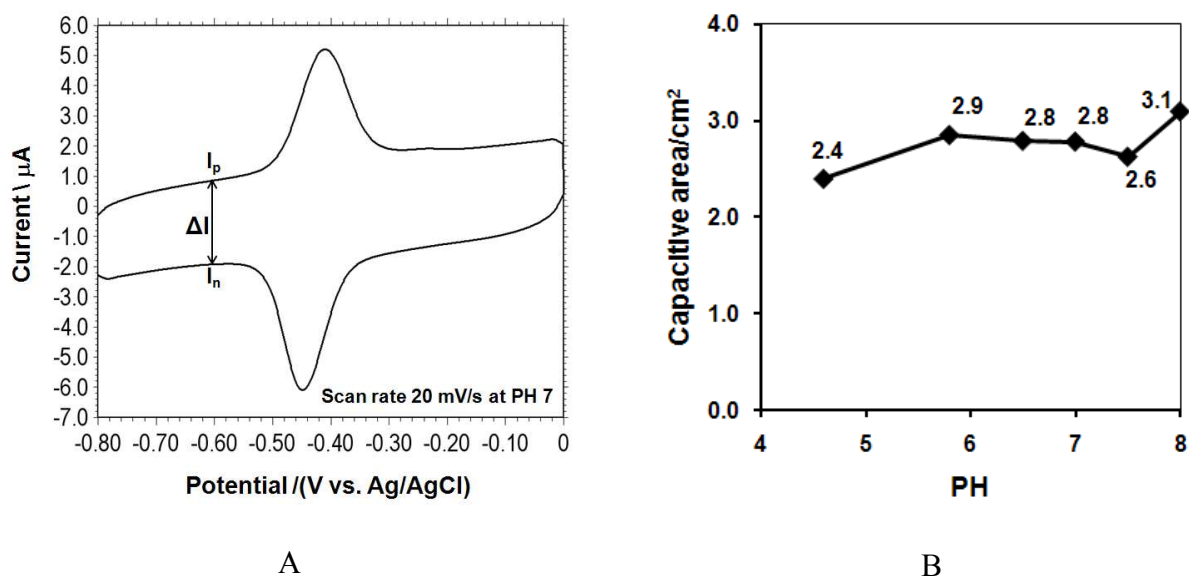


Figure S9. Panel A: A typical cyclic voltammogram of the GOx entrapped on a GC electrode coated with SWCNT/PEI matrix, the ΔI is used to calculate the capacitive area of the electrode. Panel B: Calculated capacitive areas of GOx/PEI/CNT/GC electrodes at different pH values.

For a redox couple that is immobilized on the electrode surface, the peak current is given by:

$$i_p = \frac{n^2 F^2}{4RT} v N$$

where n is the number of electrons transferred, F is Faraday's constant, v is the voltage scan rate and N is the mole of redox active sites on the surface. For GOx entrapped in CNT/PEI coated electrode and with $n=2$, one can use the slope of the linear dependence of the peak current to the scan rate (values less than 300 mV/s) to obtain the surface coverage of GOx on the electrodes. Table S1 presents the calculated GOx coverage on the electrodes for the different pH values studied. Using the GOx size dimension $6.5 \times 6.5 \text{ nm}^2$, the enzyme coverage of fully covered glassy carbon electrode is calculated to be $4 \times 10^{-12} \text{ mol/cm}^2$, two orders of magnitude less than the measured coverage. Although these data do not quantify the homogeneity or inhomogeneity of the protein's distribution on the surface, they suggest a large effective area for protein immobilization on the CNT/PEI coated electrode.

Table S1. GOx coverage of the electrodes used in pH studies

PH	Capacitive area (cm ²)	apparent coverage (pmol/cm ²)	Cap. Area coverage (pmol/cm ²)
4.6	2.4	710 ± 30	21 ± 2
5.8	2.9	680 ± 40	17 ± 3
6.5	2.8	630 ± 30	16 ± 2
7	2.8	540 ± 20	14 ± 2
7.5	2.6	450 ± 30	12 ± 1
8	3.1	330 ± 50	7.5 ± 0.3

The peak Current versus Voltage Scan Rate: In addition to the surface area estimated from the nonfaradaic charging, the peak current, i_p , was measured as a function of the voltage scan rate for electrodes coated with GOX/PEI/CNT layers and was found to exhibit a dependence that changed with the scan rates used. At low scan rates (1-300 mV/sec), a linear dependence of the peak current on the scan rates was observed; however it shifted to a more square root dependence at fast scan

rates (1000-5000 mV/sec). The data are shown for the dependence on both voltage scan rate and square root of voltage scan rate. The quality of fit measures, R-squared values of the fitting, at different scan rate ranges are shown in Table S2.

Table S2. Linear dependence factors: R-squared value of the fitting at different scan rates

0-300 mV/sec		300-800 mV/sec		1000-5000 mV/sec	
Ip-v	Ip-v ^{1/2}	Ip-v	Ip-v ^{1/2}	Ip-v	Ip-v ^{1/2}
0.998	0.980	0.996	0.997	0.975	0.997

The CV's Full Width at Half-Height (FWHH) and Formal Potential versus pH: Figure S4 shows a representative cyclic voltammogram of the GOx/SWNT/PEI modified glassy carbon electrode that was collected in a 20 mM phosphate buffer solution at pH 7. An analysis shows that the FWHH is about 80 mV for the oxidation peak and 74 mV for the reduction peak at the 10 mV/s scan rate. According to the peak separation between the oxidation and reduction, the redox reaction of the GOx is quasi-irreversible regime. Table S3 lists the FWHH values of the electrode for different pH supporting solutions.

Table S3. Full width at half height of the redox peak in different pH solutions (Averaged from two sets of data for each pH value at 10 mV/sec scan rate)

pH	4.6	5.8	6.5	7	7.5	8	7*
Oxidation	101± 2	96± 3	87± 2	80± 2	89± 2	94± 3	102± 2
Reduction	89± 3	80± 2	75± 2	73± 1	76± 2	86± 3	94± 2

* This value is for FAD immobilized at SWCNT/PEI on GC electrode; when the scan rate down to 1 mV/sec the FWHHs are 86 and 84 mV for oxidation and reduction peaks respectively.

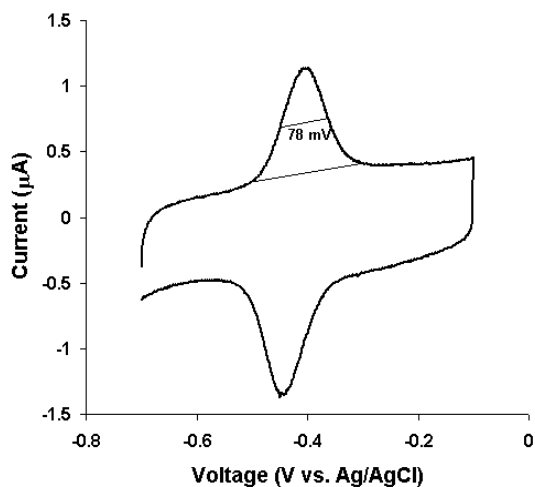


Figure S10. Characteristics of cyclic voltammogram of GOx trapped in SWCNT/PEI matrix on glassy carbon electrode

The electrochemical response of GOx immobilized onto the heterogeneous surface arises from a redox reaction of FAD, which is bound to the enzyme molecule. FAD is known to undergo a two-proton coupled two-electron transfer reaction (Eq. 1).



The full width at half height (FWHH) of the current peaks of the oxidation and reduction in the cyclic voltammograms is given by for a reversible reaction.¹

$$\Delta E_{p,1/2} = \frac{90.6}{n} \text{ mV}$$

While for an irreversible reaction it will be

$$\Delta E_{p,1/2} = \frac{62.5}{n\alpha}$$

where n is the number of electron transfer and α is symmetry factor (transfer coefficient). Using $n=2$ and ideally symmetric factor $\alpha=0.5$, one can find the FWHH to be 45.3 mV for a reversible

reaction and 62.5 mV for an irreversible reaction. The FWHH of the experimental results clearly indicate that the electron transfer can be viewed as an apparent two-electron exchange process, even though the peaks are broadened, and the pH value has a greater effect on the oxidation peak width than on the reduction wave. We note that the peak extra broadening has been normally observed for one electron transfer processes as well and ascribed to the system “non-ideality” (see also comment to Figure 1 in the main context).³

pH dependent Formal Potential: From the conclusion made above it follows that, the anodic and cathodic peak potentials of GOx immobilized on the surface of CNT should be pH dependent.

Figure S11 plots the apparent formal potential versus pH. An increase of the solution pH leads to a negative shift in potential for both anodic and cathodic peaks. The slope for a linear plot of formal potential versus pH is 52 mV/pH, which is close to the theoretical value (58.6 mV/pH) at 22 °C for a reversible, two-electron transfer reaction coupled with two proton transfer.⁴⁻⁶

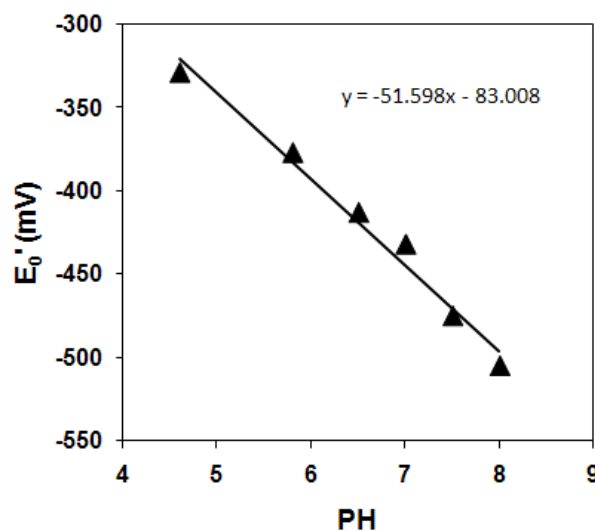


Figure S11. Formal Potential changes with the pH values

Electron Transfer Rate Constants: The dependence of the reduction (or oxidation) peak's position on the voltage scan rate can be used to characterize the electron transfer rate constant,⁷⁻⁸ and this method was applied first to determine rate constants for the glucose oxidase immobilized on the CNT/PEI films. The fitting to classical Marcus theory for the electron transfer rate constant obtained from scan rates ranging from 10 to 2000 mV/s. The theoretical curves are shown for electron transfer rate fitting with reorganization energies (λ) of 0.01, 0.3, 0.8 and 1.0 eV. A fit of the peak potential for each scan rate (i.e., one data point) yields different rate constants and reorganization energies at different scan rates. Conditionally, the “curves” represented by experimental points in Figure 3 (main context). The first region, corresponding to low scan rates, can be better fitted by theoretical curves with unrealistically low λ -s (as low as 0.01 eV), and fits still are not satisfactory. Along with the peak extra broadening, the excess peak separation (at low scan rates) Armstrong *et al.* ascribed to the systems' “non-idealities”.³ We define the electron transfer inhomogeneity factor (ETIF) as the ratio of maximum rate constant to minimum rate constant within the measured scan rates, to quantify the protein inhomogeneity at electrode surfaces under different pH values. Table S4 lists the range and average values of $\langle k^0 \rangle$ obtained from the fitting strategies under different solution conditions, and the calculated ETIF as well (see main context for discussion).

Table S4. The ranges for electron transfer rate constants obtained by fitting within the classical Marcus theory for GOx entrapped in nanotube electrodes at different pH-s

PH	4.6	5.8	6.5	7	7 (FAD)	7.5	8
k^0 Range (s^{-1})	0.22-5.7	0.29-4.5	0.38-4.3	0.45-5.4	0.35-4.3	0.45-7.0	0.34-6.0
ETIF	25.9	15.5	11.3	12.0	12.3	15.6	17.6
$\langle k^0 \rangle$ (s^{-1})	2.0±1.9	1.9±1.5	2.0±1.3	2.4±1.7	2.1±1.8	2.9±2.2	2.5±2.0

The average ET rate constants $\langle k^0 \rangle$ of “naked” FAD immobilized at GC/SWCNT/PEI is $2.1 s^{-1}$, when fitted with reorganization energy 0.3 eV, and $2.0 s^{-1}$ at 0.8 eV, somewhat slower than that of GOx.

Classical Marcus Theory and Laviron Method for temperature dependent electron transfer

rate constant: The fitting to classical Marcus theory for the electron transfer rate constant obtained from scan rates ranging from 10 to 5000 mV/s for the temperature dependent studies and the results are used in the main context discussions. As a possible alternative we used Laviron Method⁹ to calculate standard rate constants via the fitting of cyclic voltammetry data with the function of overpotential vs. $(1/m)$ value while m expressed as:

$$m = (RT/F)(k^0/nv) \quad \text{and} \quad \log(v/k^0) = \log(RT/(nFm))$$

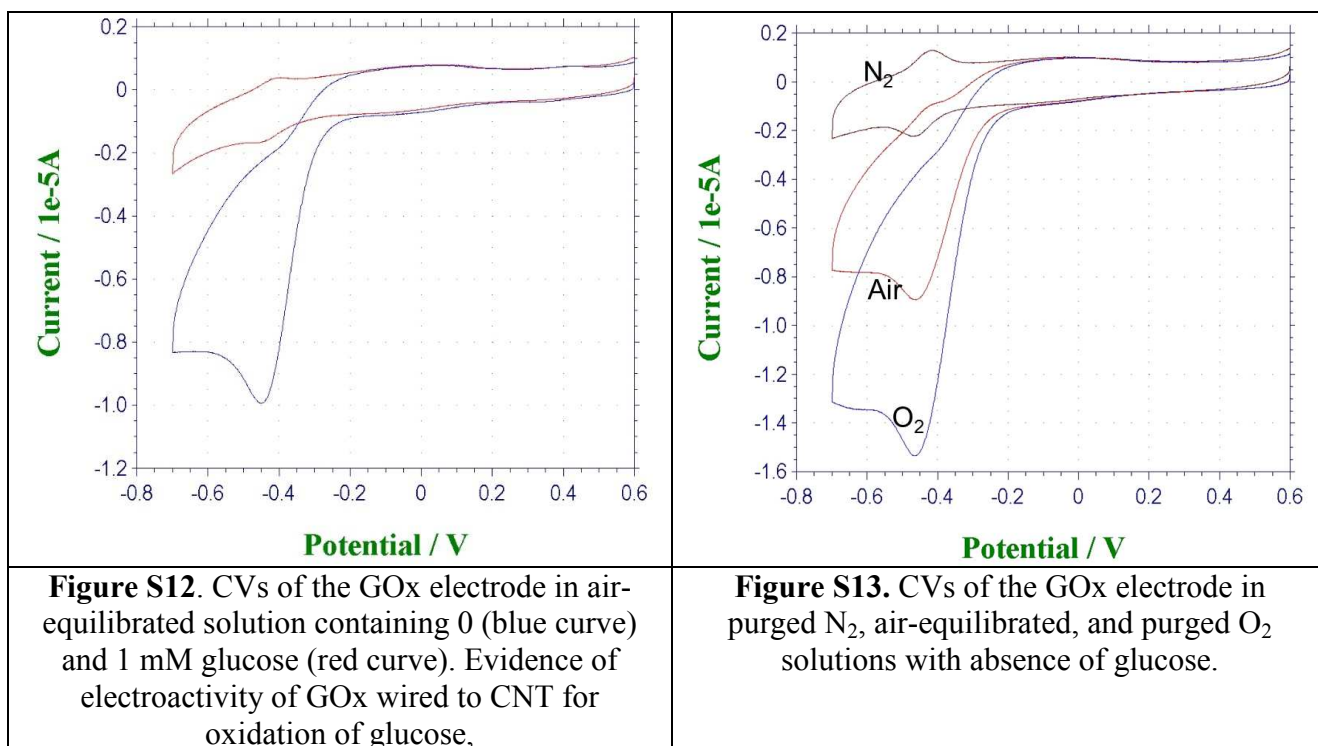
where R is gas constant, T is the temperature (absolute), n is the number of electron transfer and v is the linear voltage scan rate. Table S5 below presents rate constants of immobilized GOx calculated by using of Marcus and Laviron methods at different temperature. Laviron's method gives higher rate constant, compared to the results obtained from Marcus model.

One can see that, as in the case of the Marcus fitting, there is no uniform k^0 that can be deduced from the Laviron's model. Obviously, both, Marcus and Laviron methods are unable to account for a real situation with the Gibbs energy wells involved in the process under the consideration. However, the Marcus model, anyway dealing with curved (parabolic) Gibbs energy wells, provides some possibility of rough approximation of shallow (near-bottom) segments of actual wells (see Figure 3 in the main context, and related discussions therein). In contrast, Laviron's method is based on the Butler-Volmer theory,¹⁰ which applies solely a linear approximation to Gibbs energy wells, factually ignores (overlooks) essentially curved bottom segments of these wells and, consequently, uses CV data collected at larger scan rates (that is, at higher overvoltages). According to our analysis, this kind of data, even in the framework of the Marcus model, can not be considered as realistic, reflecting actual physical situation with Gibbs energy wells, hence the Laviron model is supposed as completely inappropriate for the application to this particular system.

Table S5. A comparison of average k^0 obtained by classical Marcus theory and Laviron method

T (K)	273	278	288	298	308	318
k^0 (s ⁻¹) (Marcus, $\lambda=0.01$ eV)	0.48	0.72	1.08	1.30	1.66	2.30
k^0 (s ⁻¹) (Marcus, $\lambda=0.8$ eV)	1.5	2.1	3.0	4.1	4.9	6.3
k^0 (s ⁻¹) (Laviron)	3.2	4.2	5.8	7.6	8.2	9.9

Control experiment on electroactivity of GOx entrapped on CNT/PEI matrix: CVs of GOx electrode with or without presence of oxygen (addendum to Figure S12-14. and to the respective discussion within the main body).



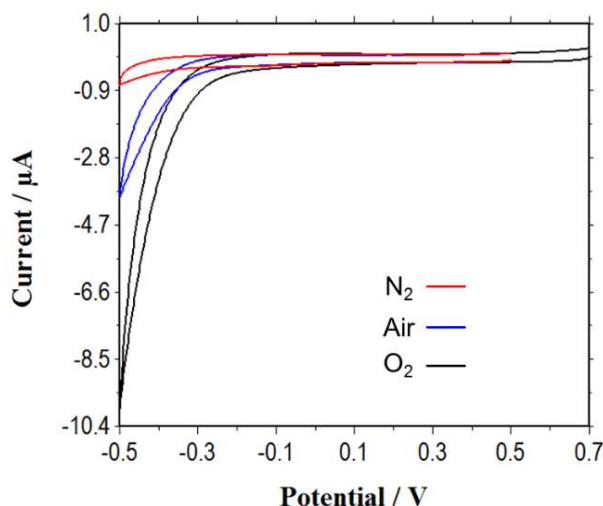
CVs of blank GC electrode in the electrolyte solution:

Figure S14. CVs of the blank GC electrode in purged N₂, air-equilibrated, and purged O₂ solutions with absence of glucose. No direct redox peaks observed at the voltage at ca. -0.45 V vs Ag/AgCl.

Presence of Hydroquinone: The electrocatalytic oxidation of glucose at different pH values has been tentatively studied by adding glucose into the electrochemical cell in the presence of 1 mM hydroquinone as an electron transfer mediator. The active electrocatalytic reaction of GOx immobilized on the GC/SWCNT/PEI electrode is evident from **Figure S15**, which shows a typical CV of a GOx/PEI/CNT/GC electrode with the addition of glucose. After addition of glucose, the anodic peak currents increase dramatically, indicating an electrocatalytic current for the oxidation of glucose. The electrocatalytic current increases with the increase of concentration of glucose in the buffer when it reaches a maximum value.

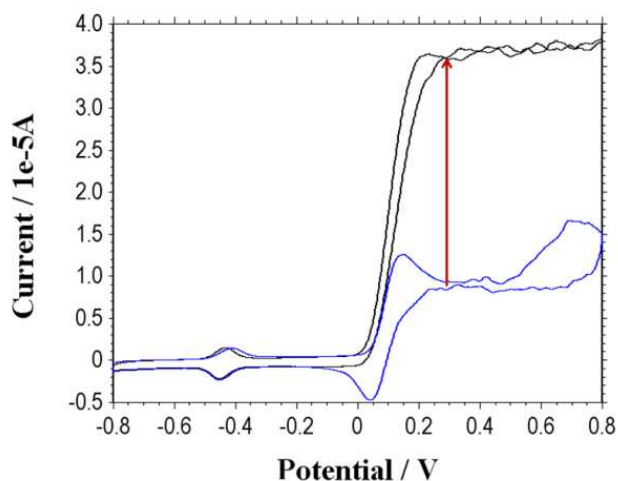


Figure S15. CV of GOx Nanocomposite electrode in the Absence (blue) and Presence (black) of Glucose, with addition of 1 mM HQ as mediator, pH 7, scan rate 10 mV/sec

References

1. Bard, A. J.; Faulkner, L. R., *Electrochemical Methods: Fundamentals and Applications*, 2nd ed.; Wiley New York, 2000.
2. Ivnitski, D.; Branch, B.; Atanassov, P.; Apblett, C., Glucose Oxidase Anode for Biofuel Cell Based on Direct Electron Transfer. *Electrochemistry Communications* **2006**, *8*, 1204-1210.
3. Armstrong, F. A.; Camba, R.; Heering, H. A.; Hirst, J.; Jeuken, L. J. C.; Jones, A. K.; Leger, C.; McEvoy, J. P., Fast Voltammetric Studies of the Kinetics and Energetics of Coupled Electron-Transfer Reactions in Proteins. *Faraday Discussions* **2000**, *116*, 191-203.
4. Hirst, J.; Duff, J. L. C.; Jameson, G. N. L.; Kemper, M. A.; Burgess, B. K.; Armstrong, F. A., Kinetics and Mechanism of Redox-Coupled, Long-Range Proton Transfer in an Iron-Sulfur Protein. Investigation by Fast-Scan Protein-Film Voltammetry. *Journal of the American Chemical Society* **1998**, *120*, 7085-7094.
5. Armstrong, F. A., Insights from Protein Film Voltammetry into Mechanisms of Complex Biological Electron-Transfer Reactions. *Journal of the Chemical Society, Dalton Transactions* **2002**, 661-671.
6. Leskovac, V.; Trivić, S.; Wohlfahrt, G.; Kandrač, J.; Peričin, D., Glucose Oxidase from *Aspergillus Niger*: The Mechanism of Action with Molecular Oxygen, Quinones, and One-Electron Acceptors. *The International Journal of Biochemistry & Cell Biology* **2005**, *37*, 731-750.
7. Tender, L.; Carter, M. T.; Murray, R. W., Cyclic Voltammetric Analysis of Ferrocene Alkanethiol Monolayer Electrode Kinetics Based on Marcus Theory. *Analytical Chemistry* **1994**, *66*, 3173-3181.

8. Weber, K.; Creager, S. E., Voltammetry of Redox-Active Groups Irreversibly Adsorbed onto Electrodes. Treatment Using the Marcus Relation between Rate and Overpotential. *Analytical Chemistry* **1994**, *66*, 3164-3172.
9. Laviron, E., General Expression of the Linear Potential Sweep Voltammogram in the Case of Diffusionless Electrochemical Systems. *Journal of Electroanalytical Chemistry and Interfacial Electrochemistry* **1979**, *101*, 19-28.
10. Pletcher, D.; Greff, R.; Peat, R.; Peter, L. M.; Robinson, J. *Instrumental Methods in Electrochemistry*. Horwood Publishing: Oxford, 2001, p.80.